Materials Transactions, Vol. 48, No. 8 (2007) pp. 2152 to 2158

Application of the Reactivity Index to Propose Intra and Intermolecular Reactivity in Metal Cluster Interaction over Oxide Surface

Abhijit Chatterjee[1] and Yoshiyuki Kawazoe[2]

[1]*Material Science, Accelrys, Tokyo 105-0003, Japan*
[2]*Institute for Materials Research, Tohoku University, Sendai 980-8577, Japan*

The hard soft acid-base (HSAB) principles classify the interaction between acids and bases in terms of global softness. In last few years the reactivity index methodology is well established and had found its application in a wide variety of systems. This study aims to propose the viability of the reactivity index to monitor metal cluster interaction with oxide surface with a description of the theory developed. We have chosen pure gold cluster from a size between 2 to 12 to be interacted with clean alumina (100) surface. The study aims to postulate a simple a priori scale in terms of intra and inter molecular interaction of gold cluster with alumina surface to rationalize the role of reactivity index in material designing. [doi:10.2320/matertrans.N-MRA2007862]

(Received December 19, 2006; Accepted May 10, 2007; Published July 19, 2007)

Keywords: *reactivity index, density functional theory, metal cluster, metal oxide, interaction, material designing*

1. Introduction

Gold is considered extremely noble. It does not oxidize and the surface of gold cannot adsorb most molecules from the gas phase.[1)] Yet it has been found that nanometer size gold particles on different oxide supports can act as catalysts even at or below room temperature.[2)] This has started a search for the factors making nanosized gold particles catalytically active. Suggestions include quantum size effects, charging of the gold particles by interaction with defects in the oxide, availability of low coordinated sites, and strain or combined effects of the gold particles and the oxide support. During the past few years, gold clusters have attracted the attention of a wide range of researchers. Apart from the fundamental understanding of the finite size effect on the physicochemical properties, the interest on gold clusters is primarily due to various applications ranging from catalysis to biological diagonistics.[3–6)] There have been a number of papers dedicated to the structure of both neutral and anionic gold clusters.[7–12)]

The hard soft acid-base (HSAB) principles classify the interaction between acids and bases in terms of global softness. Pearson proposed the global HSAB principle.[13)] The global hardness was defined as the second derivative of energy with respect to the number of electrons at constant temperature and external potential, which includes the nuclear field. The global softness is the inverse of this. Pearson also suggested a principle of maximum hardness (PMH),[14)] which states that, for a constant external potential, the system with the maximum global hardness is most stable. In recent days, DFT (Density Functional Theory) has gained widespread use in quantum chemistry. Some DFT-based local properties, *e.g.* Fukui functions and local softness, have already been used for the reliable predictions in various types of electrophilic and nucleophilic reactions.[15)] This study aims to review the development and application of reactivity index in key catalytic process within our research. The reactivity index finds its application in material designing. In our study[16)] we proposed a reactivity index scale for heteroatomic interaction with zeolite framework. The scale holds well for unisite interaction or in other way with one active site present in the molecule, the scale does not hold good for systems with two or more active sites. To overcome this limitation we derived group softness[17)] for inter and intra molecular reactivity for nitro aromatics and its adsorption over clay matrices. We as well contributed to the development of the methodology and its application in many different systems.[17–20)] The activity of nitrogen heterocyclics present in biomacromolecules and its suitable sorbent from the dioctahedral smectite family is investigated using a range of reactivity index using DFT.[21)] For the first time, a novel function λ has been defined for quantitative description of weak adsorption cases, which was so far qualitative within the domain of DFT.

DFT methods have begun its venture in oxides somewhat later but progressed in a rapid manner. In the last couple of years there have been considerable progresses in the area[22–27)] of electronic and structural properties of mixed metal oxides using first principle density functional theory. It has been proved already that, although, aluminum terminated surfaces may exist under vacuum it is likely that surfaces exposed to oxygen and water have different terminations. Jennison *et al.*[28)] have extended the work of Chambers *et al.*[29)] to a number of metals using first principle calculations and concluded that room-temperature process for creating metal-oxide interfaces discovered by Chambers on fully hydroxylated alumina, is a general phenomenon and could have many applications involving different metals. We have recently[30)] compared the silver bonding over hydroxylated alumina surface and confirmed the fact that the hydroxylated surface binds silver weakly in comparison to the clean surface and it recommends that the silver cluster over the hydroxylated surface begins to join in the formation of 3-D nuclei. The deposited Ag forms a cluster on top of the alumina surface.

With this background in the present paper, we use the reactivity index calculations on localized clusters to analyze both intramolecular and intermolecular interaction between gold clusters and oxide surface. This is to suggest that the extraordinary reactivity can be traced back to special reaction geometries available at small particles in combination with an enhanced ability of low coordinated gold atoms to interact

with the surroundings. We then present periodic density functional calculations with a range of Au cluster (as shown in the Fig. 1) starting from 2D to 3D to monitor the surface interaction of Au_n nano-particles ($n = 2$ to 12) with the alpha-alumina surface. We have performed the calculation on clean Al-terminated surface. Calculations were further performed to rationalize and validate the reason for the activity of the gold particle. The study aims to show how reactivity index can be helpful to design new materials for catalytic application.

2. Theory

The electronegativity χ, defined by Mulliken as the average of ionization potential I and electron affinity A,

$$\chi = 1/2(I + A) \tag{1}$$

is such a parameter; it is a useful measure of the tendency of a species to attract electrons. Another such conception is the idea of hardness or softness, introduced by Pearson in studying acid-base chemical reactions of the type A+ : B− = A : B, where A, the acceptor of electrons, is the acid, B, the donor of electrons, is the base. Acids and bases are classified as hard or soft. The principle of hard and soft acids and bases states that hard acids prefer to react with hard bases and soft acids prefer to react with soft bases (both thermodynamically and kinetically). This principle has been valuable for classifying a wide variety of chemical facts. Thus the electronegativity χ has been identified as the negative of the chemical potential μ, which is the Lagrange multiplier in the Euler-Lagrange equation in density functional theory, and

$$\mu = (\delta \mathrm{E}/\delta \mathrm{N})v(r) = -\chi \tag{2}$$

Where, E is the total electronic energy, N is the number of electrons, and $v(r)$ is the external electrostatic potential an electron at r feels due to the nuclei. Mulliken's formula $-1/2(I + A)$ is no more than the finite-difference approximation for eq. (1).

Which, has the finite-difference approximation $I - A$. It is remarkable that chemists sensed the importance of the quantities χ and η before their quantitative definitions as first and second derivatives of the E versus N curve were realized. The hardness/softness/acid/base principle has been derived using eq. (2) as the definition of hardness.

On the other hand, the frontier electron densities proposed by Fukui are local properties that depend on r; they differentiate one part of a molecule from another and serve as reactivity indices.

In density functional theory, hardness (η) is defined as[31)]

$$\eta = \frac{1}{2}(\delta^2 E/\delta \mathrm{N}^2)v(r) = \frac{1}{2}(\delta\mu/\mathrm{dN})_{\mathrm{v}} \tag{3}$$

Where E is the total energy, N is the number of electrons of the chemical species and the μ chemical potential.

The global softness, S, is defined as the inverse of the global hardness, η.

$$\mathrm{S} = 1/2\eta = (\delta \mathrm{N}/\delta\mu)_{\mathrm{v}} \tag{4}$$

Using the finite difference approximation, S can be approximated as

$$\mathrm{S} = 1/(\mathrm{IE} - \mathrm{EA}) \tag{5}$$

where IE and EA are the first ionization energy and electron affinity of the molecule, respectively.

The Fukui function $f(r)$ is defined by[32)]

$$f(r) = [\delta\mu/\mathrm{dv}(r)]_{\mathrm{N}} = [\delta\rho(r)/\delta \mathrm{N}]_{\mathrm{v}} \tag{6}$$

The function 'f' is thus a local quantity, which has different values at different points in the species. Since $\rho(r)$ as a function of N has slope discontinuities, eq. (1) provides the following three reaction indices:[32)]

$$f^-(r) = [\delta\rho(r)/\delta N]_{\mathrm{v}}{}^- \text{ (governing electrophilic attack)}$$
$$f^+(r) = [\delta\rho(r)/\delta N]_{\mathrm{v}}{}^+ \text{ (governing nucleophilic attack)}$$
$$f^0(r) = \frac{1}{2}[f^+(r) + f^-(r)] \text{ (for radial attack)}$$

In a finite difference approximation, the condensed Fukui function[31)] of an atom, say x, in a molecule with N electrons are defined as:

$$f_{\mathrm{x}}{}^+ = [q_{\mathrm{x}}(N + 1) - q_{\mathrm{x}}(N)] \text{ (for nucleophilic attack)} \tag{7}$$
$$f_{\mathrm{x}}{}^- = [q_{\mathrm{x}}(N) - q_{\mathrm{x}}(N - 1) \text{ (for electrophilic attack)}$$
$$f_{\mathrm{x}}{}^0 = [q_{\mathrm{x}}(N + 1) - q_{\mathrm{x}}(N - 1)]/2 \text{ (for radical attack)}$$

where q_{x} is the electronic population of atom x in a molecule. The local softness $s(r)$ can be defined as

$$s(r) = (\delta\rho(r)/\delta\mu)_{\mathrm{v}} \tag{8}$$

Equation (3) can also be written as

$$s(r) = [\delta\rho(r)/\delta \mathrm{N}]v[\delta \mathrm{N}/\delta\mu]_{\mathrm{v}} = f(r)S \tag{9}$$

Thus, local softness contains the same information as the Fukui function $f(r)$ plus additional information about the total molecular softness, which is related to the global reactivity with respect to a reaction partner, as stated in HSAB principle. Atomic softness values can easily be calculated by using eq. (4), namely:

$$s_{\mathrm{x}}{}^+ = [q_{\mathrm{x}}(\mathrm{N} + 1) - q_{\mathrm{x}}(N)]S \tag{10}$$
$$s_{\mathrm{x}}{}^- = [q_{\mathrm{x}}(N) - q_{\mathrm{x}}(N - 1)]S$$
$$s_{\mathrm{x}}{}^0 = S[q_{\mathrm{x}}(\mathrm{N} + 1) - q_{\mathrm{x}}(N - 1)]/2$$

We further explained the interaction energy scheme as follows. This is known that A & B interacts in two steps: (1) interaction will take place through the equalization of chemical potential at constant external potential and (2) A and B approach the equilibrium state through changes in the electron density of global system generated by making changes in the external potential at constant chemical potential. That means within DFT we can write

$$\Delta E_{\mathrm{inter}} = E[\rho\mathrm{AB}] - E[\rho\mathrm{A}] - E[\rho\mathrm{B}] \tag{11}$$

Where ρAB, ρA, ρB are the electron densities of the systems AB at equilibrium and of the isolated systems A and B, respectively.

Or in terms of the potentials we can write

$$\Delta E_{\mathrm{inter}} = \Delta E_{\mathrm{v}} + \Delta E_{\mu}$$

Where, $\Delta E_{\mathrm{v}} = -1/2[(\mu_{\mathrm{A}} - \mu_{\mathrm{B}})^2/(S_{\mathrm{A}} + S_{\mathrm{B}})]\ (S_{\mathrm{A}}S_{\mathrm{B}})$

$$\Delta E_\mu = -1/2 N_{AB}{}^2 k[1/(S_A + S_B)$$

N_{AB} total no. of electrons, k the proportionality constant between S_{AB} and $S_A + S_B$, product of N^2 and K is λ.

$$\Delta E_\mu = (-1/2)\lambda/(S_A + S_B)$$

If the interaction is taking place through j site of A,

$$\lambda_{Aj} = q_{Aj}{}^{eq} - q_{Aj}{}^{0} \quad (12)$$

$q_{Aj}{}^{eq}$ is density of jth atom of A in complex AB & $q_{Aj}{}^{0}$ is the density in isolated system.
This new definition proved to be more accurate while proposing the interactions, in compared to the well established interaction energy.

3. Method and Model

Ab initio total energy pseudopotential calculations were performed using CASTEP (Cambridge Serial Total Energy Package) and associated programs for symmetry analysis, which has been described elsewhere.[33,34] In this code, the wave functions of valence electrons are expanded in a basis set of plane waves with kinetic energy smaller than a specified cutoff energy, E_{cut}. The presence of tightly bound core electrons is represented by nonlocal ultrasoft pseudopotentials.[35] CASTEP is a pseudopotential total energy code that employs Perdew and Zunger[36] parameterization of the exchange-correlation energy, super cells and special point integration over the Brillouin zone and a plane wave basis set for the expansion of wave functions. Becke-Perdew parameterization[37,38] of the exchange-correlation functional, which includes gradient correction (GGA), was employed. The pseudoptentials are constructed from the CASTEP database. Reciprocal space integration over the Brilloin zone is approximated through a careful sampling at a finite number of k points using the Monkhorst-Pack scheme.[39] Here we used symmetric 5 k-points In all calculations. The basis cutoff used is 380.0 eV. The energy tolerance is 5.0×10^{-6} eV/atom, the force tolerance is 0.01 eV/Å, and the displacement tolerance is 5.0×10^{-4} Å. To obtain equilibrium structures for a given set of lattice constants, ionic and electronic relaxations were performed using the adiabatic or 'Born-Oppenheimer' approximation, where the electronic system is always in equilibrium with the ionic system. Relaxations were continued until the total energy had converged. Total energy calculations were performed on a supercell with periodic boundary conditions, which enables us to use a basis of plan waves. The supercell has the form of a rhombohedral prism, and in the stoichiometric slab it contains 30 atoms. This slab is exactly the thickness of one bulk unit cell of the corundum structure. $2 \times 2 \times 4$ unit cell is used for all slab calculations. The slabs are separated by a vacuum layer of 10–12 Å which is sufficient to keep interaction between the slabs negligible even after deposition of clusters. The clusters are placed approximately 3 Å above the alumina surface. Figure 1 shows the structure with labeled atoms. The slab was hydroxylated on one surface. The opposite side of the slab was kept frozen at positions for the surface. This is necessary since a bulk-terminated surface is not stable due to its large surface dipole, which causes very large relaxations to occur[30] on this surface, which consists of 3 O-ions per unit cell and one Al-ion slightly above the O-plane. The gold clusters were optimized within the same periodic boundary condition applied as used for the alumina slab model.

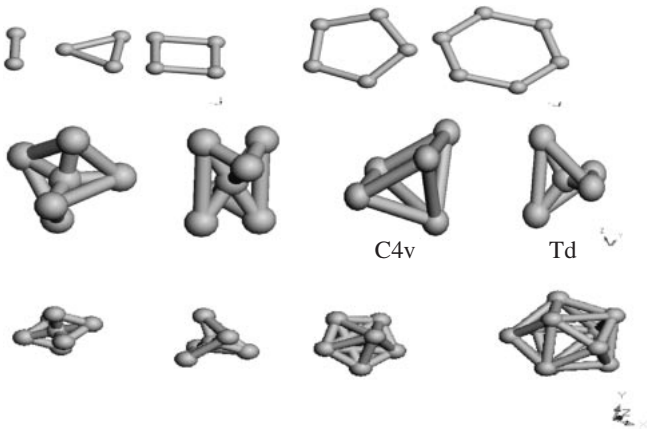

Fig. 1 Few of the representative gold clusters Au_m ($m = 2$ to 12) used in this study. We have used two different symmetries for only Au5 cluster as labeled in the figure c4V and Td respectively.

In the current study, all calculations with molecular boundary conditions have been carried out with DFT[40–43] using DMol3 code of Accelrys. A gradient corrected functional BLYP[44,45] and DNP basis set[46] was used through out the calculation. Basis set superposition error (BSSE) was also calculated for the current basis set in nonlocal density approximation (NLDA). Single point calculations of the cation and anion of each molecule at the optimized geometry of the neutral molecule were also carried out to evaluate Fukui functions and global and local softness. The condensed Fukui function and atomic softness were evaluated using eqs. (7) and (9), respectively. The gross atomic charges were evaluated by using the technique of electrostatic potential (ESP) driven charges.

4. Results and Discussion

4.1 Electronic structure and binding energy of Au_m clusters (where $m = 2$ to 12).

We here have used different starting geometries were used for each cluster size, with no symmetric constrains imposed. We have concentrated on spin multiplicities. Only relaxed geometries in the lowest spin multiplicity were investigated. Fukui functions and reactivity was calculated using ESP derived charges. We have compared the situation with and without gold cluster over clean alumina surface. The clusters are shown in Fig. 1, we have as well shown an example in case of a Au5 cluster that there is possibility to have different symmetry again within the 3D structures which may certainly influence the nature of the binding of these clusters, which is certainly beyond the scope of the current paper. We have plotted the binding energy per atom vs. cluster size in Fig. 2. The binding energy per atom is calculated using the expression

$$EB = [ET - mEatom]/m \quad (13)$$

Where, m is the number of atoms present in the gold cluster.

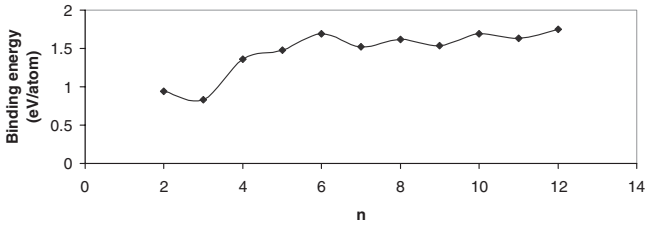

Fig. 2 The relation between binding energy/atom vs. gold cluster Au_n ($n = 2$ to 12) size as n.

The results are shown in Fig. 2. The results show that three is a bit oscillation but for Au_n clusters we see a general increase in binding energy until Au6. There is small dip at Au6 then the increment in binding energy is monotonic until Au12. The trend matches with that of Chiranjib *et al.*[11] They have predicted that clusters are planar until Au = 6. We have find the same behavior with an exception with cases where symmetric constrains were applied. This rationalizes the fact that binding energy for small gold clusters increases in general with some exceptions. Now it is crucial to see how they interact with the support. It is as well needed to validate that whether the clusters remain active after binding on the oxide surface to behave catalytically, which may tell us about the comparative activity of 2D and 3D gold clusters. We also see at this point that smaller cluster until 6 is highly planar if symmetric constrain is withdrawn. The clusters with bigger size have lesser flexibility.

4.2 Reactivity index calculation on localized clusters to predict activity trend in presence and absence of alumina cluster

Our aim is to rationalize the structure of gold cluster over α-Al_2O_3 (001). We have performed the calculation on clean Al-terminated surface. First we loaded gold with increasing size from $m = 2$ to 12, with various possibility of 2D and 3D gold cluster to calculate binding energy for the lowest energy conformer. We wish to analyze the origin of this effect through the reactivity of gold cluster to bond with the surface and to still remain active for further catalytic reaction.

To explain the activity of the gold clusters with or without the oxide support we have decided to look this phenomenon through localized reactivity index numbers. This will help us to propose both intra and intermolecular interaction probability within the cluster and as well during their interaction with oxide surface. To mimic the oxide surface we have designed a cluster with a structural formula of Al_8O_{12} as shown in Fig. 3(a). To represent an infinite surface with a cluster is a challenge and we designed the cluster to mimic the local environment to be extrapolated infinitely within a periodic domain. We have used the pure clusters shown in Fig. 1 and put them over the alumina cluster as shown in Figs. 3(b) and 3(c) respectively representing situations where alumina cluster is interacting with Au5 at two different symmetry. The goal is to see the effect of the pure gold clusters and if they have some change in terms of activity when interacted with alumina surface. This the best way to do that, as this will be more scalable as we are looking at both intra and inter atomic interaction between the cluster atoms

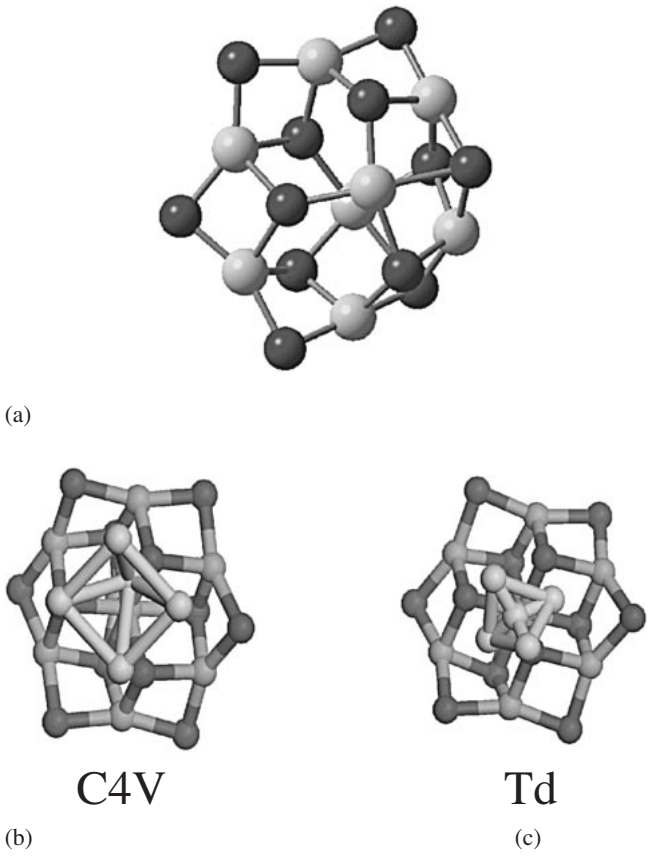

Fig. 3 (a) The optimized geometry of the cluster representing alumina with formula Al_8O_{12}; (b) The optimized adsorption complex of alumina cluster and Au5 cluster with c4V symmetry; (c) The optimized adsorption complex of alumina cluster and Au5 cluster with Td symmetry.

and their interaction with alumina surface mimicked by the cluster. The Fukui function and local softness for the hydroxyl proton is presented both in terms of nucleophilic and electrophilic activity. Roy *et al.*[46] have introduced relative electrophilicity (s_x^+/s_x^-) and relative nucleophilicity (s_x^-/s_x^+). These can be defined as the electrophilicity of any site as compared to its own nucleophilicity for the first term and vice versa. The site with highest (s_x^+/s_x^-) is the most probable site to be attacked by a nucleophile, and the site having the highest (s_x^-/s_x^+) ratio is the most probable site to be attacked by an electrophile. We have successfully used this parameter for both intermolecular and intramolecular interaction. The results for Fukui function, local softness both in terms of nucleophilicity and electrophilicity as well the relative nucleophilicity trend is shown in Table 1 and Table 2 for pure cluster and for the cluster while interacted with alumina cluster, respectively. From the results of Table 1 it is observed that as expected the global softness increases with the size of the gold cluster. The relative electrophilicity decreases with increase in the cluster size. That means that intra molecular interaction decreases with increase in cluster size as also justified by localized directive Fukui function numbers from the same table. Now, let us look into the situation while the gold clusters are interacting with the alumina cluster. The global softness increases as usual, forecasting that in intermolecular interaction one should look for short range interactions. The relative electro-

Table 1 Fukui function, local softness and relative nucleophilicity for the gold cluster Au_n ($n = 2$ to 12) pure.

M	S	f_x^+	s_x^+	f_x^-	s_x^-	s_x^+/s_x^-	s_x^-/s_x^+
Au5(Td)	2.45	0.15	0.36	0.016	0.039	9.23	0.30
Au5(C4V)	2.41	0.12	0.31	0.017	0.041	7.56	0.67
Au6	2.69	0.21	0.56	0.030	0.081	6.91	0.14
Au7	2.74	0.23	0.63	0.043	0.117	5.38	0.18
Au8	2.82	0.25	0.70	0.047	0.132	5.30	0.19
Au9	2.91	0.30	0.87	0.052	0.151	5.76	0.17
Au10	3.01	0.33	0.99	0.055	0.150	5.66	0.15
Au11	3.21	0.39	1.25	0.061	0.196	5.37	0.16
Au12	3.43	0.43	1.98	0.063	0.216	5.17	0.11

Table 2 Fukui function, local softness and relative nucleophilicity for the gold cluster Au_n ($n = 2$ to 12) while interacting with alumina surface cluster.

M	S	f_x^+	s_x^+	f_x^-	s_x^-	s_x^+/s_x^-	s_x^-/s_x^+
Au5(Td)	2.45	0.25	0.61	0.066	0.161	3.79	0.26
Au5(C4V)	2.41	0.22	0.53	0.059	0.142	3.73	0.27
Au6	2.69	0.19	0.51	0.043	0.115	4.43	0.22
Au7	2.74	0.17	0.46	0.041	0.112	4.11	0.24
Au8	2.82	0.21	0.59	0.039	0.110	5.36	0.19
Au9	2.91	0.24	0.70	0.035	0.102	6.86	0.15
Au10	3.01	0.27	0.81	0.031	0.093	8.71	0.11
Au11	3.21	0.31	0.99	0.027	0.086	11.51	0.09
Au12	3.43	0.34	1.17	0.023	0.078	15.00	0.07

philicity really produces a very opposite trend with alumina clusters. The activity is increasing with the size now, which is just opposite to the trend for the pure gold cluster activity. This proposes that the clusters with bigger size will remain active after adsorbing over alumina surface. We surely need to do some magic number clusters to propose something more realistic. But at this point two things are clear the smaller 2D cluster remain unstable compared to 3D while the clusters are interacting with alumina surface. As well it says that, with increase in size the gold remains active even after adsorption over the alumina surface. We may need to perform some reactions over them to quantify the mechanism.

4.3 Electronic structure of (001) surface of α-Al_2O_3 with and without gold cluster deposition using periodic models.

The (001) surface of α-Al_2O_3 has a layered structure as shown in Fig. 4. In which each oxygen plane in the bulk has an associated Al plane at a distance of 0.838 Å above and below, forming a stoichiometric triple layer. The most convenient unit cell is a rhombohedral prism comprising three such (001) oxygen planes separated by the associated pairs of Al planes. The oxygen planes are separated by 2.166 Å and form a hexagonal lattice with ABABAB... stacking. Their positions are slightly laterally distorted from ideal hexagonal sites. The Al atoms occupy two-thirds of the octahedral holes in the oxygen sub lattice, at the positions, which alternate between below and above the centers of these holes. The unoccupied octahedral holes are themselves stacked on a face centered cubic lattice, ABCABC. A C3v symmetry axis passes through each Al atom and through the

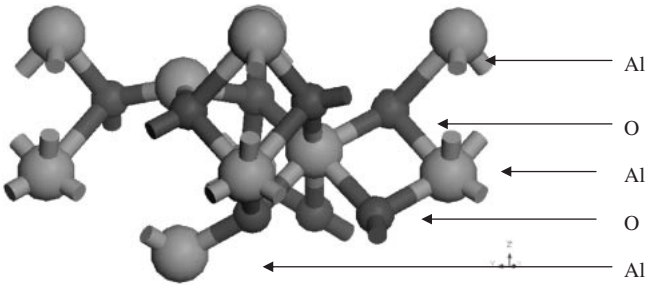

Fig. 4 The periodic slab model representing α-Al_2O_3 with all the atoms labeled. The bottom two layers were fixed throughout the calculation.

centers of the unoccupied octahedral sites. The stoichiometric slab has two equivalent surfaces, which are terminated by an Al plane, as in Fig. 1. The termination defines the stoichiometric surface, because the slab as a whole is stoichiometric and has two equivalent surfaces.

We first optimized the aluminum lattice and the energy value is calculated using GGA (Table 3). The results for Al-terminated surface are in match with the numbers generated by Wang *et al.*[47] and Batirev *et al.*[48] It is observed that the planar relaxations are quite large, while the O ions and the Al ions remain essentially coplanar within ~0.02 Å. The relaxation of surface Al is accompanied by a 9% reduction in the length of bond (1.687 Å) to the second layer oxygen, which is less than the experimental value of ~4%.[40] The reduction is a natural consequence of the reduced coordination of surface Al. Coordination with the outermost O atoms also causes a shortening of bonds to interior Al neighbors (1.804 Å and 1.889 Å). These reductions result in part for the small lateral displacements within the O layer, which

Table 3 The total energy, binding energy and the interaction energy in terms of reactivity index as obtained for alumina lattices.

Component	Total energy Kcal/mol	BE (eV)	λ (eV)
Al_2O_3	−2932.226		
Au(Td)	−421.14		
Au(C4V)	−420.67		
Al_2O_3 + Au(Td)	−3367.164	−4.31	−2.79
Al_2O_3 + Au(C4V)	−3366.134	−3.91	−1.41

manifest them primarily as slight distortions and rotations of the triangles of O atoms below each surface Al. The predicted lateral displacement pattern qualitatively matches with the experimental values.[47)]

We loaded the clusters over alumina optimized surface. We have shown example of the optimized geometry for the two specific symmetry clusters representing Au5 clusters over alumina surface in Fig. 5(a) and (b) respectively. After each loading of gold clusters, the upper three layers of the structure including the gold are optimized. The total energy of the isolated system along with the system including adsorbed gold; and their binding energy with each loading is studied and has been shown in Table 3 for the two symmetry groups only. The binding energy for metals over the alumina surface is calculated as the following:

$$E_{\text{binding}} = (ME_{\text{metal}} + E_{\text{Slab}} - E_{\text{total}})/M$$

Where E_{binding} is the binding energy per metal atom binded to the alumina surface, E_{metal} is the energy of isolated metal atom, M is the number of metal atoms, E_{Slab} is the energy of the slab and E_{total} is the total energy of the metal adsorbed alumina system. Hence the binding energy is defined as positive if the total energy decreases when the metal atom is brought from infinity and placed onto the surface. We have as well calculated the interaction energy (λ) in terms of which is based on reactivity at a certain external potential within a specific chemical potential. The numbers are shown in Table 3, the trend produced by both the binding energy and interaction energy is same. We will follow this up with bigger clusters to validate, which is the plan for the future study.

4.4 Comparison of two methodologies

We have used tow methodologies to monitor the interaction of gold clusters with alumina slab. With our background with the theory and application of reactivity index in different system the current study aims to explore the area of metal clusters and its interaction with oxide surface within the domain of reactivity index. We have shown successfully that the reactivity index can identify the localized interaction probability of the gold clusters with alumina surface mimicked by a localized cluster. To validate this we have performed the binding energy calculation using slab model, the trend very well matches with the reactivity index trend. We further extrapolated our derived interaction energy calculation methodology through λ and the results are comparable. Hence this study could show that reactivity index can be successfully applicable to the metal cluster and its interaction with oxide surface.

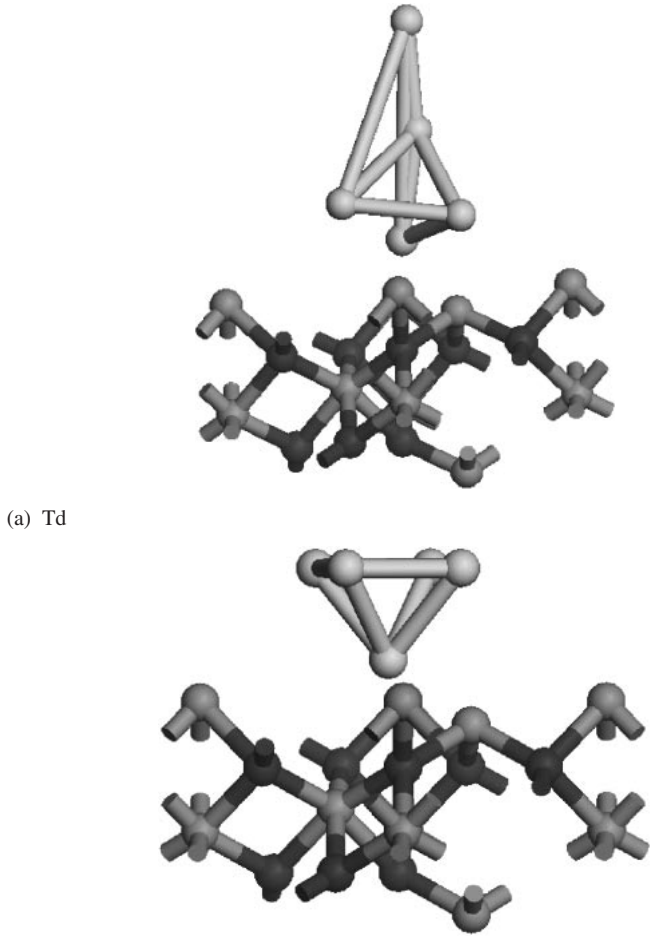

(a) Td

(b) C4v

Fig. 5 (a) The structure of clean α-Al_2O_3 with Au5 at c4V symmetry after optimization. (b) The structure of clean α-Al_2O_3 with Au5 at Td symmetry after optimization. The bottom two layers were fixed throughout the calculations.

5. Conclusion

This is a first systematic study to look into the interaction of gold clusters with alumina surface. We have systematically first compared the binding energy for the gold clusters, which are very close to the trends of other *ab initio* calculations. Then we put those clusters to interact with alumina surface to figure out their interaction capability both at intra and intermolecular level, a very interesting trend is observed to justify two things. First smaller 2D clusters are not stable over alumina surface. The reactivity index and specially the relative reactivity indices show a steady decrease in the nucleophilicity with increase in the size of the cluster. The trend was very different when the Au_n cluster interacted with the alumina surface the nucleophilicity increases for bigger clusters, showing the predominant role of support. This explains why gold remain active after attaching with the support. There is a marked difference between the orbital contribution with change of symmetry and is observed at isolated system and during interaction for Au5 cluster (Td and C4V). The interaction energy result can as well be validated by the λ parameter and proves its credibility. This study as well validates the range of reactive

index, it has been so far successfully applied to many other systems, but the current study successfully opens up the door for reactivity to penetrate in the area of metal cluster. Last but not the least to bring more meaningful conclusion we certainly need to look into the size of the cluster, which we wish to pursue in the future.

REFERENCES

1) B. Hammer and J. K. Nørskov: Nature **376** (1995) 238–243.
2) M. Haruta: Catal. Today **36** (1997) 153–162.
3) T. G. Schaaff and R. L. Whetten: J. Phys. Chem. B **104** (2000) 2630–2641.
4) H. Häkkinen, M. Moseler and U. Landman: Phys. Rev. Lett. **89** (2002) 033401–033404.
5) J. G. Hou, B. Wang, J. Yang, X. R. Wang, H. Q. Wang, Q. Zhu and X. Xiao: Phys. Rev. Lett. **86** (2001) 5321–5324.
6) C. J. Kiely, J. Fink, M. Brust, D. Bethell and D. J. Schiffrin: Nature **396** (1998) 444–447.
7) K. Balasubramanian and D.-W. Liao: J. Chem. Phys. **94** (1991) 5233–5239.
8) G. Bravo-Perez, I. L. Garzon and O. Navarro: Chem. Phys. Lett. **313** (1999) 655–659.
9) J. Wang, G. Wang and J. Zhao: Phys. Rev. B **66** (2002) 035418–035423.
10) H. Häkkinen and U. Landman: Phys. Rev. B **62** (2000) R2287–R2290.
11) R. M. Olson, S. Varganov, M. S. Gordon, H. Metiu, S. Chretien, P. Piecuch, K. Kowalski, S. A. Kucharski and M. Musial: J. Amer. Chem. Soc. **127** (2005) 1049–1052.
12) C. Majumder and S. K. Kulshrestha: Phys. Rev. B **73** (2006) 155427–155437.
13) R. G. Parr and R. G. Pearson: J. Am. Chem. Soc. **105** (1983) 7512–7516.
14) R. G. Pearson: J. Chem. Educ. **64** (1987) 561–567.
15) P. Geerlings and F. De Proft: Int. J. Quant. Chem. **80** (2000) 227–235.
16) A. Chatterjee, T. Iwasaki and T. Ebina: J. Phys. Chem. A **103** (1999) 2489–2494.
17) A. Chatterjee, T. Iwasaki, T. Ebina and F. Mizukami: J. Chem. Phys. **118** (2003) 10212–10220.
18) A. Chatterjee, Y. Onodera, T. Ebina and F. Mizukami: J. Mol. Graphics & Modeling **22** (2003) 93–104.
19) A. Chatterjee, T. Suzuki, Y. Onodera and D. A. P. Tanaka: Chemistry—A European Journal **9** (2003) 3920–3929.
20) A. Chatterjee, Y. Onodera, T. Ebina and F. Mizukami: J. Chem. Phys. **120** (2004) 3414–3424.
21) A. Chatterjee, T. Iwasaki and T. Ebina: J. Phys. Chem. A **105** (2001) 6187–6196.
22) A. Asthagiri and D. S. Sholl: J. Chem. Phys. **116** (2002) 9914–9925.
23) J. A. Rodriguez, S. Azad, LQ, Wang, J. Garcia and A. Etxeberria: J. Chem. Phys. **118** (2003) 6562.
24) D. C. Sorescu and J. T. Jr. Yates: J. Phys. Chem. B **106** (2002) 6184–6199.
25) J. A. Snyder, D. R. Alfonso, J. E. Jaffe, Z. Lin, A. C. Hess and M. Gutowski: J. Phys. Chem. B **104** (2000) 4717–4722.
26) A. Asthagiri and D. S. Sholl: Surface Science **581** (2005) 66–87.
27) J. A. Rodriguez, J. C. Hanson, S. Chaturvedi, A. Maiti and J. L. Brito: J. Phys. Chem. B **104** (2000) 8145–8152.
28) D. R. Jennison and T. R. Mattsson: Surface Science **544** (2003) L689–L696.
29) S. A. Chambers, T. Droubey, D. R. Jennison and T. R. Matsson: Science **297** (2002) 827–831.
30) A. Chatterjee, S. Niwa and F. Mizukami: Journal of Molecular Graphics and Modelling **23** (2005) 447–456.
31) W. Yang and W. J. Mortier: J. Am. Chem. Soc. **108** (1986) 5708–5711.
32) R. G. Parr and W. T. Yang: J. Am. Chem. Soc. **106** (1984) 4049–4050.
33) M. P. Teter, M. C. Payne and D. C. Allen: Phys. Rev. B **40** (1989) 12255–12263.
34) M. C. Payne, M. P. Teter, D. C. Allen, T. A. Arias and J. D. Johannopoulos: Rev. Modern. Phys. **64** (1992) 1045–1097.
35) D. Vanderbilt: Phys. Rev. B **41** (1990) 7892–7895.
36) J. Perdew and A. Zunger: Phys. Rev. B **23** (1981) 5048–5079.
37) J. P. Perdew: Phys. Rev. B **33** (1986) 8822–8824.
38) A. D. Becke: Phys. Rev. A **38** (1988) 3098–3100.
39) H. J. Monkhorst and J. D. Pack: Phys. Rev. B **13** (1976) 5188–5192.
40) B. Delley: J. Chem. Phys. **92** (1990) 508–517.
41) B. Delley: J. Chem. Phys. **94** (1991) 7245–7250.
42) B. Delley: J. Chem. Phys. **113** (2000) 7756–7764.
43) B. Delley: *Modern Density Functional Theory: A Tool for Chemistry*; J. M. Seminario, P. Politzer, Eds., Theoretical and Computational Chemistry, Vol. 2, (Elsevier Science: Amsterdam, 1995).
44) A. D. Becke: J. Chem. Phys. **88** (1988) 2547–2553.
45) C. T. Lee, W. T. Yang and R. G. Parr: Physical Review B. **37** (1988) 785–789.
46) R. K. Roy, S. Krishnamurti, P. Geerlings and S. Pal: J. Phys. Chem. A **102** (1998) 3746–3755.
47) Y. Wang, X.-G. Wang, A. Chaka and M. Scheffer: Phys. Rev. Lett. **81** (2000) 1038–1041.
48) I. G. Batirev, A. Alavi, M. W. Finnis and T. Deutsch: Phys. Rev. Lett. **82** (1999) 1510–1513.